Journal of Mechanics in Medicine and Biology
Vol. 11, No. 2 (2011) 273–284

DOI: 10.1142/S0219519411004034

World Scientific
www.worldscientific.com

DIRECT NUMERICAL SIMULATION OF DETACHMENT OF SINGLE CAPTURED LEUKOCYTE UNDER DIFFERENT FLOW CONDITIONS

Z. Y. LUO*,†, F. XU†,‡, T. J. LU† and B. F. BAI*,†,§

*State Key Laboratory of Multiphase Flow in Power Engineering
Xi'an Jiaotong University, Xi'an 710049, China

†Biomedical Engineering and Biomechanics Center
SV Laboratory, School of Aerospace, Xi'an Jiaotong University
Xi'an 710049, P. R. China

‡HST-Center for Biomedical Engineering, Department of Medicine
Brigham and Women's Hospital, Harvard Medical School
Boston, MA, USA
§bfbai@mail.xjtu.edu.cn

Received 15 January 2011
Accepted 15 January 2011

Antibody-based cell isolation using microfluidics finds widespread applications in disease diagnostics and treatment monitoring at point of care (POC) for global health. However, the lack of knowledge on underlying mechanisms of cell capture greatly limits their developments. To address this, in this study, we developed a mathematical model using a direct numerical simulation for the detachment of single leukocyte captured on a functionalized surface in a rectangular microchannel under different flow conditions. The captured leukocyte was modeled as a simple liquid drop and its deformation was tracked using a level set method. The kinetic adhesion model was used to calculate the adhesion force and analyze the detachment of single captured leukocyte. The results demonstrate that the detachment of single captured leukocyte was dependent on both the magnitude of flow rate and flow acceleration, while the latter provides more significant effects. Pressure gradient was found to represent as another critical factor promoting leukocyte detachment besides shear stress. Cytoplasmic viscosity plays a much more important role in the deformation and detachment of captured leukocyte than cortex tension. Besides, better deformability (represented as lower cytoplasmic viscosity) noteworthy accelerates leukocyte detachment. The model presented here provides an enabling tool to clarify the interaction of target cells with functional surface and could help for developing more effective POC devices for global health.

Keywords: Single captured leukocyte; detachment; microfluidics; level set method.

§Corresponding author.

1. Introduction

To alleviate the severe situation of the global burden of diseases, antibody (Ab)-based capture method to separate blood bioparticles using microfluidics has been widely used to create point-of-care (POC) systems for disease diagnostics and treatment monitoring, offering the potential of minimized device size and maximized cost effectiveness. Accordingly, this method has been utilized to separate and enumerate various blood bioparticles (as biomarkers) for different diseases, such as CD4+T-cells and virus particles for HIV,[1–3] circulating tumor cells for cancers.[4,5] Although significant advances have been made in different areas related to Ab-based capture method such as finding of more specific Abs[6] and improved design of microfluidic devices,[7] there still exists an unmet need for POC devices with improved capture efficiency and specificity. Therefore, there is an urgent need to understand the underlying mechanism of Ab-based capture method using microfluidics.

Experimental studies have shown that there exists an optimal flow condition for maximizing capture efficiency, which varies with the types of target bioparticles.[3,5,8,9] Generally, flow condition determines the contact duration between target bioparticles and Abs on a functionalized surface, which affects the capture efficiency. After capture, the flow induced hydrodynamic forces (e.g., shear stress, drag force, and lift force during washing process) still push captured bioparticles and may separate them form Abs, indicating the dependence of capture efficiency on the detachment of captured bioparticles. However, the detachment of captured bioparticles has only been studied recently.[10–12] Zhang *et al.*[10] observed the attachment and detachment of four types of cells on functional surfaces modified by three different reagents. Then, the detachment of captured cancer cells was found to be affected by flow acceleration.[11] More recently, a threshold for shear stress to detach cancer cell was studied through microfluidic experiments.[12] Although these three studies developed statistical phenomenal models to fit their experimental data, the physical mechanisms of the detachment behaviors of captured bioparticles are still unknown and urgently need to be studied.

As compared to experimental studies, mathematical modeling of Ab-based bioparticles capture using microfluidics is favorable since it is easy-to-control and cost effective.[13,14] Various theoretical models have been developed. For instance, several models (e.g., capsule model,[15–17] and compound drop model[18–22]) have been developed to simulate the cell deformation.[14] Some adhesion models (e.g., adhesion kinetic model[18,21,23] and stochastic simulation systems[16,17,22]) integrating kinetics of adhesion bonds have been used to calculate adhesion force and simulate cell adhesion kinetics. These theoretical models have provided insight into the behaviors of cell deformation, adhesion, and rolling on functionalized surfaces. However, study on the detachment of captured cells has not yet been systematically applied.

In the present study, we developed a mathematical model, integrating a level set method to track leukocyte deformation, to study the detachment of single captured leukocyte on a functionalized surface in a rectangular microchannel under different

flow conditions. We focused on the leukocyte that is an important biomarker for human immune system. Computational methods used were described in Sec. 2. Effects of several factors (including flow rate, flow acceleration, and leukocyte properties) on the detachment of single captured leukocyte were studied and discussed in Sec. 3.

2. Computational Methods

2.1. *Leukocyte model and flow configuration*

The detachment of single captured leukocyte was studied by employing the parabolic flow (the typical flow pattern in microfluidics) in a rectangular microchannel (Fig. 1). The captured leukocyte was considered as a simple liquid drop rounded by a cortex with a constant tension T_c. The drop model maintains certain rheological properties of leukocytes in spite of its simplicity. The drop divides whole fluid system to two parts, i.e. plasma around the leukocyte and cytoplasm in the leukocyte, whose density and viscosity are ρ_0, μ_0 and ρ_1, μ_1, respectively. The leukocyte is placed in the middle of computational domain and has an initial contact area l_0 with bottom functionalized surface. The computational domain, with length L_c and height H_c, is labeled by solid line grid (Fig. 1(a)). The simulating flow system is placed in an XY coordinate system where the main flow direction along the two parallel flat plates is set as positive direction of X-axis and Y-axis points to upper plate vertically.

2.2. *Kinetic adhesion model*

To calculate the total adhesion force, kinetic adhesion model developed by Dembo *et al.*[24] was employed. The model considers single bond as a Hookean spring.

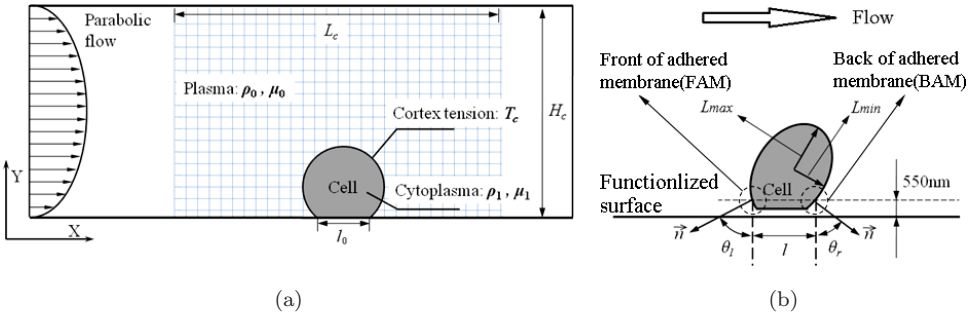

(a) (b)

Fig. 1. Illustration of problem statement: (a) the cell is modeled as a simple liquid drop with constant cortex tension; the lattice area is computational domain with length L_c and height H_c; contact area of the cell is denoted by l (l_0 denotes initial area) and (b) schematic illustration of some parameters.

Accordingly, adhesion force f_b (N) produced by single adhesion bond and the total adhesion force F_b (N) can be computed by

$$f_b = \sigma(l_x - l_{mv} - \lambda) \quad F_b = N_b f_b, \tag{1}$$

where σ (N/m) is spring constant, l_x(m) is the distance between leukocyte membrane and functionalized surface, l_{mv} (m) is microvillus length (Fig. 2(a)), λ (m) is unstressed bond length, and N_b (m^{-2}) is bond density. According to reversible chemical reaction theory,[25] N_b is deduced from adhesion kinetic equation, which controls the balance between formation and dissociation of adhesion bonds, as follow[24]:

$$\frac{\partial N_b}{\partial t} = k_f(N_{l0} - N_b)(N_{r0} - N_b) - k_r N_b, \tag{2}$$

where N_{l0} (m^{-2}) is the initial ligand density on functionalized surface andN_{r0} (m^{-2}) is the initial receptor density on leukocyte membrane. k_f (m^2/s) and k_r (s^{-1}) are forward and reverse reaction rates that are calculated by[24]

$$k_f = k_f^0 \exp\left(-\frac{\sigma_{ts}(l_x - l_{mv} - \lambda)^2}{2kT}\right) \quad k_r = k_r^0 \exp\left(\frac{(\sigma - \sigma_{ts})(l_x - l_{mv} - \lambda)^2}{2kT}\right), \tag{3}$$

where k_f^0 (m^2/s) and k_r^0 (s^{-1}) are initial forward and reverse reaction rate, k is Boltzmann constant, T (K) is absolute temperature, and σ_{ts} (N/m) is spring constant of adhesion bonds at transition state (the state of adhesion bonds changing from slip bonds to catch bonds). Parameter values used in this theoretical model are shown in Table 1.

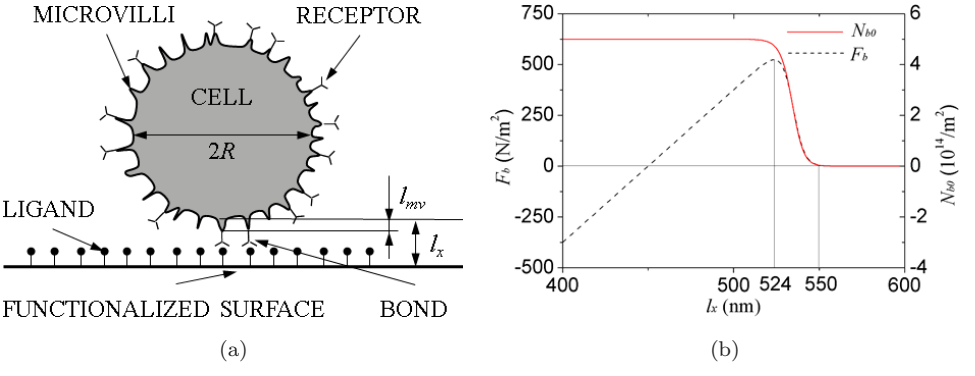

Fig. 2. Illustration of relationship between l_x and l_{mv} and variation of total adhesion force F_b. (a) Schematic illustration of bond length. Because only receptors on microvillus tips can interact with ligands, the length of adhesion bond is $l_x - l_{mv}$. (b) Equilibrium bond density N_{b0} and total adhesion force F_b calculated from kinetic adhesion model vary as the function of l_x. Total adhesion force reaches the largest value when $l_x = 524$ nm, and when $l_x > 550$ nm and F_b becomes approximately zero.

Table 1. Parameter values used in this article.

Parameter	Definition	Range	References	Value used
R (μm)	Leukocyte radius	3.5–7	[20, 28]	6.5
L_c (μm)	Length of computational domain	50	[18, 20]	$8R$
H_c (μm)	Height of computational domain	10–100	[11, 17, 18, 20, 21, 23]	$4R$, $6R$, $8R$
ρ_0 (kg/m^3)	Plasma density	1000	[28]	1000
μ_0 (Pa $\cdot$ s)	Plasma viscosity	0.0008–0.001	[16, 17, 22]	0.0008
$\lambda_\rho = \rho_1/\rho_0$	Density ratio	1.06–1.10	[28]	1.0
$\lambda_\mu = \mu_1/\mu_0$	Viscosity ratio	10–10000	[28]	75, 50, 20
T_c (μN/m)	Cortical tension	20–35	[28]	20, 30, 35
N_{l0} (m^{-2})	Initial ligand density	$(0.2–5.0)\times10^{15}$	[20, 31, 32]	2.5×10^{16}
N_{r0} (m^{-2})	Initial receptor density	$(0.02–5.0)\times10^{16}$	[20, 31, 32]	5.0×10^{14}
k_{f0} (m^2/s)	Initial forward reaction rate	10^{-18}–10^{-10}	[33]	10^{-10}
k_{r0} (s^{-1})	Initial reverse reaction rate	10^{-5}–10	[33]	10
σ (N/m)	Spring constant	10^{-5}–10^{-2}	[33]	1.5×10^{-5}
σ_{ts} (N/m)	Transition spring constant	$(5.0–9.5)\times10^{-3}$	[33]	1.0×10^{-4}
l_{mv} (μm)	Unstressed microvillus length	0.30–0.35	[16–18, 20–22]	0.35
λ(μm)	Unstressed bond length	0.01–0.1	16–18, 20–22	0.1
k (N $\cdot$ m/K)	Boltzmann constant	1.38×10^{-23}	[18, 21]	1.38×10^{-23}
T (K)	Temperature	310.0	[18, 21]	310.0

There exists an equilibrium adhesion bond density N_{b0} (m^{-2}) for each l_x. N_{b0} can be calculated by setting the time-dependent term in Eq. (2) as zero. Then, two solutions[21] (N_1, N_2) can be got as:

$$N_{1,2} = \frac{\left(N_{l0} + N_{r0} + \dfrac{k_r}{k_f}\right) \pm \sqrt{\left(N_{l0} + N_{r0} + \dfrac{k_r}{k_f}\right)^2 - 4N_{l0}N_{r0}}}{2}. \tag{4}$$

The larger solution (N_1) is not realistic because its value is larger than possible number of available bonds (less than N_{l0} and N_{r0}), which means $N_{b0} = N_2$.

As shown by Jin *et al.*,[21] a characteristic time (t_c) is used to determine whether to consider variation of N_b over time. t_c can be computed by

$$t_c = [k_f(N_1 - N_{b0m})]^{-1}, \tag{5}$$

where N_{b0m} is the maximum value of N_b calculated from Eq. (4) when $k_r = k_{r0}, k_f = k_{f0}$. For parameter values used in this article, t_c represents O(10^{-7}) (s). When shear rate is great as 10000 s^{-1}, the characteristic flow time is only O(10^{-4}) (s) but much larger than t_c. Accordingly, N_b equals to N_{b0} meaning that F_b is only the function of l_x.

Then, variations of N_b and F_b as l_x are represented in Fig. 2(b). F_b reaches the maximum when $l_x = 524$ nm. When $l_x > 550$ nm, F_b becomes approximately zero.

Accordingly, in the following discussion, the specific cell membrane only contributes to adhesion area l when l_x is lower than the critical value 550 nm (Fig. 1(b)).

2.3. *Governing equations and boundary conditions*

When employing level set method to capture leukocyte membrane, the conservation of mass and momentum of incompressible flow system can be described by governing equations as follow:

$$\begin{aligned} \nabla \cdot v &= 0 \\ \frac{\partial v}{\partial t} + \nabla \cdot (vv) &= \frac{\nabla p}{\rho_x} + \frac{\nabla \cdot [\mu_x \nabla v + \mu_x (\nabla v)^T]}{\rho_x \mathrm{Re}} - \frac{\kappa(\phi)\delta_\varepsilon(\phi)\nabla\phi}{\rho_x \mathrm{We}} + \frac{\delta_\varepsilon(\phi)\nabla\phi}{\rho_x \mathrm{Ad}} \\ \frac{\partial \phi}{\partial t} + v \cdot \nabla\phi &= 0, \end{aligned} \tag{6}$$

where v and p are dimensionless velocity vector and pressure field. Equation (6) has been normalized by characteristic velocity, length, and time as U_0 (centerline velocity of initial inlet flow), R, and R/U_0. ϕ is the level set function assumed to be the distance from the interface, $\kappa(\phi)$ is surface curvature, $\delta_\varepsilon(\phi)$ is delta function, $\rho_x = \lambda_\rho + (1-\lambda_\rho)H_\varepsilon(\phi)$ and $\mu_x = \lambda_\mu + (1-\lambda_\mu)H_\varepsilon(\phi)$, where $\lambda_\rho = \rho_1/\rho_0, \lambda_\mu = \mu_1/\mu_0$, and $H_\varepsilon(\phi)$ are Heaviside functions.[26] Nondimensional parameters are Reynolds number $\mathrm{Re} = \rho_0 U_0 R/\mu_0$, Weber number $\mathrm{We} = \rho_0 U_0^2 R/T_c$, Adhesion number $\mathrm{Ad} = \rho_0 U_0^2/F_b$, which are respectively presenting the ratios of the inertia force to the viscous force, the surface tension, and the adhesion force.

No-slip boundary condition is employed at the top and bottom planes and a periodic boundary condition is employed in X-axis direction to reduce the size of computational domain and time. Governing equations are solved by using a three-stage RKCN four-step projection method.[26,27] The details of numerical resolutions can be found in our research.[28]

Computational results are presented below based on dimensionless parameters normalized by characteristic velocity U_0, length R, and time R/U_0. For example, the time $t^* = t/(R/U_0)$, initial adhesion area $l_0^* = l_0/R$, the change rate of adhesion area $(dl/dt)^* = d(l/R)/dt^*$, and flow acceleration $a^* = d(U_t/U_0)/dt^*$(U_t is centerline velocity of inlet flow at any time). To track leukocyte deformation, deformation index is defined as $D^* = (L_{\max} - L_{\min})/(L_{\max} + L_{\min})$, where $L_{\max}$ and $L_{\min}$ are the maximum and minimum radius of the ellipsoidal leukocyte. Definitions of other parameters are represented in Fig. 1(b).

3. Results and Discussion

3.1. *Validation of numerical method*

To validate the numerical method used, first, we simulated the leukocyte deformation in linear shear flow without considering adhesion force and compared the simulation results with previous numerical results.[29,30] We observed a good qualitative

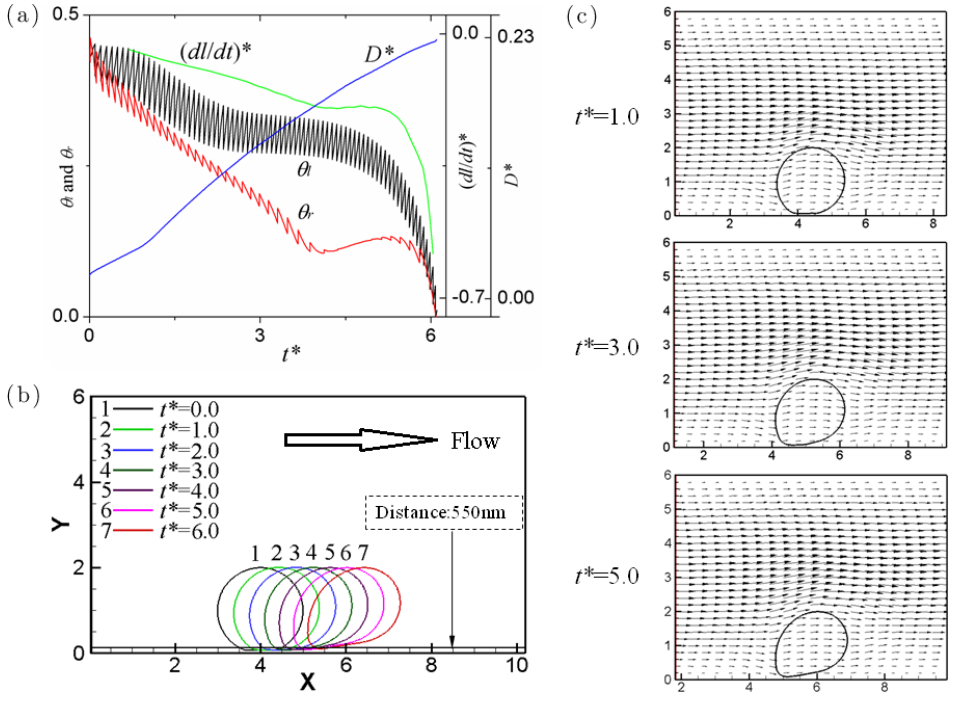

Fig. 3. The deformation and detachment of captured leukocyte at Re = 6.5, We = 138.7, $\lambda_\mu = 50$, and $l_0^* = 0.875$: (a) changes of D^*, $(dl/dt)^*$, θ_l, and θ_r as functions of dimensionless time t^*; (b) the shape of captured leukocyte changes as the time t^*; and (c) velocity vector of whole flow field at different time t^*.

agreement. The details of methodology validation are presented in our previous research.[28]

We analyzed the detachment of captured leukocyte (Fig. 3). After grid independence test, the mesh with 321×241 elements is used for computational domain of $8R \times 6R$. Besides, leukocyte volume is tracked and changes less than -0.25% from its initial volume. θ_l and θ_r are defined as Fig. 1(b) to track changes of adhesion area. Since surrounding fluid pushes the leukocyte (Fig. 3(c)), θ_l increases until the grid element of adhesion area separates and θ_r decreases until new grid element of adhesion area forms. Thus, the change frequency of θ_l and θ_r reflect separating and forming rate of the front and back of adhered leukocyte membrane (defined in Fig. 1(b) and abbreviated as FAM and BAM in latter discussion). Shown in Fig. 3(a), the separating rate of FAM keeps almost unchanged, but the forming rate of BAM decreases until it becomes approximately zero. It leads the change rate of adhesion area $(dl/dt)^*$ decreases until leukocyte detachment reaches a steady state. In parabolic velocity field, captured leukocyte would be elongated by surrounding fluid[19] and its front and back are elongated in the form of paraboloid and plane,[20] which is also represented by our results (Figs. 3(b) and 3(c)). Increasing rate of deformation index D^* (reflecting elongation of the leukocyte) is found to decrease

(Fig. 3(a)). It probably results from the existence and development of a thin region of high pressure between leukocyte membrane and functionalized surface, which is observed in our simulation and in the paper of Liu *et al.*[19] This high-pressure region is also probably leading to the decrease of forming rate of BAM (Fig. 3(a)). Besides, leukocyte inclination angle between $L_{\max}$ and X-axis is found to decrease (Fig. 3(b)); it is identified by previous work.[18] Under the cooperation of hydrodynamic force provided by surrounding fluid and adhesion force provided by functionalized surface, the leukocyte rolls and slides on functionalized surface, which was also observed by Jin *et al.*[21]

3.2. *Effects of flow conditions*

First, we performed simulation of the detachment of captured leukocyte with different initial adhesion areas (Fig. 4(a)). We observed that the detachment

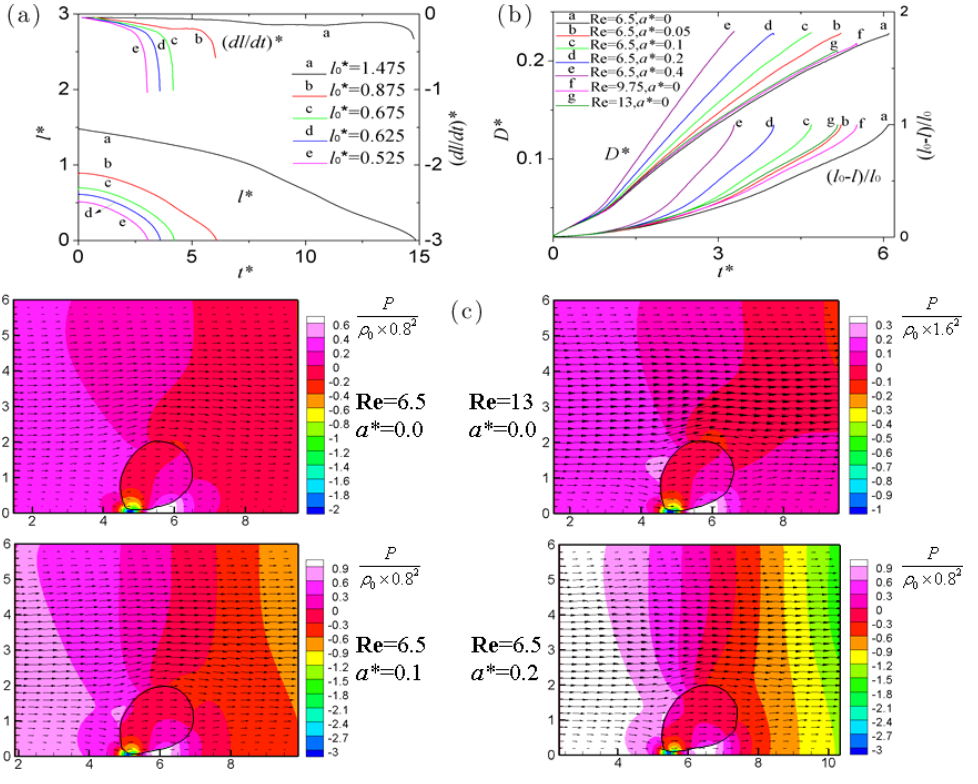

Fig. 4. Detachment and deformation of single captured leukocyte under different flow conditions: (a) adhesion area l^* and its change rate $(dl/dt)^*$ vary as functions of t^* when initial adhesion area varies at $\mathrm{Re} = 6.5$, $\mathrm{We} = 138.7, \lambda_\mu = 50$; (b) deformation index and adhesion area $(l_0 - l)/l_0$ (normalized by its initial value l_0) are functions of t^* under different flow conditions when $l_0^* = 0.875, \mathrm{We} = 138.7, \lambda_\mu = 50$; and (c) velocity vector and dimensionless pressure $(P/(\rho_0 U_0^2))$ contour under different flow conditions when $t^* = 4.0$.

speed of leukocyte increases with decreasing adhesion area. When adhesion area is larger, total adhesion force counteracting hydrodynamic forces turns stronger because of the existence of more adhesion bonds. Increases of total adhesion force decelerate leukocyte detachment. If initial adhesion area is too small (i.e. $l_0^* = 0.525, 0.625, 0.675$), the leukocyte detaches so rapidly that it has separated completely before its detachment reaches the steady state. Accordingly, the value of l_0^* is fixed at 0.875 in latter simulations to ensure the steady state of leukocyte detachment, but l_0^* is not fixed at 1.475 to save computing time.

We also studied the changes of adhesion area and deformation index under different flow conditions (Fig. 4(b)). Shear stress has been considered the most important factor in leukocyte detachment.[12] According to our results, we observed that leukocyte detachment at constant velocity conditions (CVCs) speeds up, as velocity value U_0 increases (which enlarges shear rate, Fig. 4(c)). It identifies that the increase of shear stress (proportional to shear rate) accelerates leukocyte detachment. However, we also found pressure gradient is another nonignorable factor of leukocyte detachment, which even has more significant influences than shear stress. In Fig. 4(b), as flow acceleration increasing at flow acceleration conditions (FACs), the leukocyte deforms and separates much more speedily. Even if the velocity U_t during the whole separating process at FAC (i.e. $\mathrm{Re} = 6.5, a^* = 0.1, 0.2$) keeps smaller than that at CVC (i.e. $\mathrm{Re} = 13, a^* = 0.0$), the detachment and deformation of the leukocyte are strengthened much more significantly in the former case. Accordingly, shear rate keeps smaller at FAC than that at CVC, but pressure gradient keeps larger which results in much stronger fluid drag force in main-stream direction (it reinforces separation of FAM). In addition, the increase of flow acceleration enlarges gradient magnitude of the high-pressure region beneath the back of captured leukocyte (Fig. 4(c)). It decelerates the forming of BAM, even possibly induces BAM to detach instead. Besides, the high-pressure region probably increases lift force on the leukocyte to accelerate leukocyte leaving.

3.3. *Effects of cortex tension and cytoplasmic viscosity*

According to our previous research,[28] leukocyte deformability is determined by We and λ_μ (representing roles of cortex tension and cytoplasmic viscosity). Figure 5 illustrates their effects on detachment and deformation of captured leukocyte. We observed that λ_μ has more significant influence on leukocyte deformability than We (Fig. 5(a)). Cytoplasmic fluidity (the ability to flow) increases with increasing λ_μ, implying that leukocyte rigidity is considerably strengthened with increasing cytoplasmic viscosity. Small change of We (from 208.0 to 118.9) almost applies no effect on leukocyte deformation when $\lambda_\mu = 50, 75$ (Fig. 5(a)). Shown in Fig. 5(a), the increase of deformability (i.e. λ_μ decreases from 75 to 20) accelerates leukocyte detachment. It performs more remarkably before leukocyte detachment reaches the steady state. The main reason is probably that larger deformation induces the leukocyte to get closer to the region of higher shear rate (Fig. 5(b)). Besides,

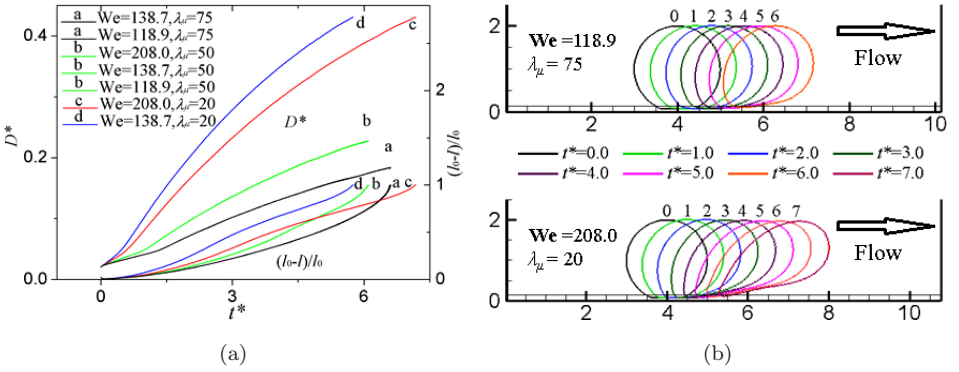

(a) (b)

Fig. 5. Effects of leukocyte properties including cortex tension and viscosity ratio: (a) changes of D^* and adhesion area $(l_0 - l)/l_0$ are presented, when $l_0^* = 0.875$ and Re = 6.5, with different leukocyte properties and (b) changes of leukocyte shape.

favorable deformability (i.e. $\lambda_\mu = 50, 20$) is conductive to leukocyte creep causing much higher separating rate of FAM. However, we observed that small λ_μ (i.e. $\lambda_\mu = 20$) extends the leukocyte separation time (Fig. 5(a)). Under this condition, the leukocyte undergoes significant deformation near the contact region, where leukocyte membrane is stretched just like a tremendous microvilli to prevent the leukocyte separating (Fig. 5(b)). We also found, when cytoplasmic viscosity is small (i.e. $\lambda_\mu = 20$), separating rate increases with increasing cortex tension before and during the steady state of leukocyte detachment (Fig. 5(a)). Cortex tension applied on adhered leukocyte membrane points away from the functionalized surface thus exacerbates the departure of adhered membrane. On the other hand, greater cortex tension leads to smaller deformation near the contact region, and weakens the contribution of the specific extended leukocyte membrane on preventing leukocyte detachment.

4. Conclusions

In this article, a mathematical model integrating a level set method with adhesion kinetic model was developed to simulate the detachment of single captured leukocyte on functionalized surface. We considered three factors including flow velocity, cell properties (i.e., cortex tension, cytoplasmic viscosity), and flow acceleration. A steady state of separating rate was observed in leukocyte detachment. A higher flow velocity can accelerate leukocyte detachment at CVCs, but the separating rate increases more significantly under FACs. Comparing leukocyte detachment under CVCs and that under FACs, pressure gradients were found to affect leukocyte detachment much more significantly than the shear stress. In addition, smaller cytoplasmic viscosity (i.e. $\lambda_\mu = 50, 20$) induces the leukocyte to deform more easily and separate more speedily, but the separation time of captured leukocyte extends

if λ_μ is too small as 20. Compared to cytoplasmic viscosity, cortex tension provides much less influence on leukocyte detachment, and its effects can be observed only when λ_μ is small as 20. These findings are very helpful for controlling leukocyte detachment behaviors in microfluidics and improving capture efficiency of functionalized microchannels to create Ab-based POC systems for global health.

Acknowledgments

The financial support of the XJTU Foundation for interdisciplinary research (2009xjtujc04) is gratefully acknowledged. T.J.L. and F.X. were supported by the National Natural Science Foundation of China (10825210, 10632060), the National 111 Project of China (B06024), and the National Basic Research Program of China (2006CB601201, 2006CB601202).

References

1. Kim YG, Moon S, Kuritzkes DR, Demirci U, Quantum dot-based HIV capture and imaging in a microfluidic channel, *Biosens Bioelectron* **25**:253–258, 2009.
2. Moon S, Keles HO, Ozcom A, Khademhosseine A, Hæggstrom D, Kuritykes D, Demirci U, Integrating microfluidics and lensless imaging for point-of-care testing, *Biosens Bioelectron* **24**:3208–3214, 2009.
3. Cheng XH, Irimia D, Dixon M, Sekine K, Demirci U, Zamir L, Tompkins RG, Rodriguez W, Toner M, A microfluidic device for practical label-free CD4+ T-cell counting of HIV-infected subjects, *Lab Chip* **7**:170–178, 2007.
4. Adams AA, Okagbare PI, Feng J, Hupert ML, Patterson D, Gottert J, McCarley RL, Nikitopoulos D, Murphy MC, Soper SA, Highly efficient circulating tumor cell isolation from whole blood and label-free enumeration using polymer-based microfluidics with an integrated conductivity sensor, *J Am Chem Soc* **130**:8633–8641, 2008.
5. Nagrath S, Sequist LV, Maheswaran S, Bell DW, Irimia D, Ulkus L, Smith MR, Kwak EL, Digumarthy S, Muzikansky A, Ryan P, Balis UJ, Isolation of rare circulating tumour cells in cancer patients by microchip technology, *Nature* **450**:1235-U10, 2007.
6. Phillips JA, Xu Y, Xia Z, Fan ZH, Tan WH, Enrichment of cancer cells using aptamers immobilized on a microfluidic channel, *Anal Chem* **81**:1033–1039, 2009.
7. Cheng XH, Gupta A, Chichen C, Tompkins RG, Rodriguez W, Toner M, Enhancing the performance of a point-of-care CD4+ T-cell counting microchip through monocyte depletion for HIV/AIDS diagnostics, *Lab Chip* **9**:1357–1364, 2009.
8. Sin A, Murthy SK, Revzin A, Tompkins RG, Toner M, Enrichment using antibody-coated microfluidic chambers in shear flow: model mixtures of human lymphocytes, *Biotechnol Bioeng* **91**:816–826, 2005.
9. Murthy SK, Sin A, Tompkins RG, Toner M, Effect of flow and surface conditions on human lymphocyte isolation using microfluidic chambers, *Langmuir* **20**:11649–11655, 2004.
10. Zhang X, Jones P, Haswell SJ, Attachment and detachment of living cells on modified microchannel surfaces in a microfluidic-based lab-on-a-chip system, *Chem Eng J* **135**:S82–S88, 2008.
11. Cheung LSL, Zheng XG, Stopa A, Baygents JC, Guzman R, Schroeder JA, Heimark RL, Zohar Y, Detachment of captured cancer cells under flow acceleration in a biofunctionalized microchannel, *Lab Chip* **9**:1721–1731, 2009.

12. Couzon C, Duperray A, Verdier C, Critical stresses for cancer cell detachment in microchannels, *Eur Biophys J Biophys Lett* **38**:1035–1047, 2009.
13. Verdier C, Couzon C, Duperray A, Singh P, Modeling cell interactions under flow, *J Math Biol* **58**:235–259, 2009.
14. Lim CT, Zhou EH, Quek ST, Mechanical models for living cells — a review, *J Biomech* **39**:195–216, 2006.
15. Sukumaran S, Seifert U, Influence of shear flow on vesicles near a wall: a numerical study, *Phys Rev E* **64**, 2001.
16. Jadhav S, Eggleton CD, Konstantopoulos K, A 3-D computational model predicts that cell deformation affects selectin-mediated leukocyte rolling, *Biophys J* **88**: 96–104, 2005.
17. Pappu V, Doddi SK, Bagchi P, A computational study of leukocyte adhesion and its effect on flow pattern in microvessels, *J Theor Biol* **254**:483–498, 2008.
18. Khismatullin DB, Truskey GA, A 3D numerical study of the effect of channel height on leukocyte deformation and adhesion in parallel-plate flow chambers, *Microvasc Res* **68**:188–202, 2004.
19. Liu XH, Wang X, The deformation of an adherent leukocyte under steady shear flow: a numerical study, *J Biomech* **37**:1079–1085, 2004.
20. Khismatullin DB, Truskey GA, Three-dimensional numerical simulation of receptor-mediated leukocyte adhesion to surfaces: effects of cell deformability and viscoelasticity, *Phys Fluids* **17**:21, 2005.
21. Jin Q, Verdier C, Singh P, Aubry N, Chotard-Ghodsnia R, Duperray A, Migration and deformation of leukocytes in pressure driven flows, *Mech Res Comm* **34**:411–422, 2007.
22. Pappu V, Bagchi P, 3D computational modeling and simulation of leukocyte rolling adhesion and deformation, *Comput Biol Med* **38**:738–753, 2008.
23. N'Dri NA, Shyy W, Tran-Soy-Tay R, Computational modeling of cell adhesion and movement using a continuum-kinetics approach, *Biophys J* **85**:2273–2286, 2003.
24. Dembo M, Torney DC, Saxman K, Hammer D, The reaction-limited kinetics of membrane-to-surface adhesion and detachment, *Proc R Soc Lond B Biol Sci* **234**: 55–83, 1988.
25. Kramers HA, Brownian motion in a field of force and the diffusion model of chemical reactions, *Physica* **7**:284–304, 1940.
26. Ni MJ, Abdou M, Komori S, A variable-density projection method for interfacial flows, *Numer Heat Trans B Fund* **44**:553–574, 2003.
27. Ni MJ, Komori S, Morley N, Projection methods for the calculation of incompressible unsteady flows, *Numer Heat Trans B Fund* **44**:533–551, 2003.
28. Luo ZY, Xu F, Lu TJ, Bai BF, Direct numerical simulation of single leukocyte deformation in microchannel flow for disease diagnosis, *J Med Syst*, DOI: 10.1007/s10916-010-9502-3, 2010.
29. Ramanujan S, Pozrikidis C, Deformation of liquid capsules enclosed by elastic membranes in simple shear flow: large deformations and the effect of fluid viscosities, *J Fluid Mechan* **361**:117–143, 1998.
30. Lac E, Barthes-Biesel D, Deformation of a capsule in simple shear flow: effect of membrane prestress, *Phys Fluids* **17**:8, 2005.
31. Bell GI, Models for the specific adhesion of cells to cells, *Science* **200**:618–627, 1978.
32. Vonandrian UH, Hasslen SR, Nelson RD, Erlandsen SL, Butcher EC, A central role for microvillous receptor presentation in leukocyte adhesion under flow, *Cell* **82**:989–999, 1995.
33. Bell GI, Dembo M, Bongrand P, Cell adhesion: competition between nonspecific repulsion and specific bonding, *Biophys J* **45**:1051–1064, 1984.